Geophysical Journal International

Geophys. J. Int. (2022) **228,** 1281–1293
Advance Access publication 2021 September 24
GJI Seismology

https://doi.org/10.1093/gji/ggab392

Mayotte seismic crisis: building knowledge in near real-time by combining land and ocean-bottom seismometers, first results

Jean-Marie Saurel[1], Eric Jacques,[1] Chastity Aiken[2], Anne Lemoine[3], Lise Retailleau,[1,4] Aude Lavayssière,[1] Océane Foix,[2] Anthony Dofal[1,5], Angèle Laurent,[1] Nicolas Mercury,[3,6] Wayne Crawford,[1] Arnaud Lemarchand,[1] Romuald Daniel,[1] Pascal Pelleau,[2] Maxime Bès de Berc,[6] Grégoire Dectot,[7] Didier Bertil,[3] Agathe Roullé,[3] Céleste Broucke,[8] Alison Colombain,[3] Hélène Jund,[8] Simon Besançon,[1] Pierre Guyavarch,[2] Philippe Kowalski,[1,4] Mickaël Roudaut,[2] Ronan Apprioual,[2] Jean Battaglia,[9] Soumya Bodihar,[1] Patrice Boissier,[1,4] Marie Paule Bouin,[1] Christophe Brunet,[1,4] Kévin Canjamale,[1,4] Philippe Catherine,[1,4] Nicolas Desfete,[1,4] Cécile Doubre,[6] Rémi Dretzen,[8] Tom Dumouche,[1] Philippe Fernagu,[2] Valérie Ferrazzini,[1,4] Fabrice R. Fontaine,[1,5] Arnaud Gaillot,[2] Louis Géli,[2] Cyprien Griot,[1,4] Marc Grunberg,[8] Emre Can Guzel,[10] Roser Hoste-Colomer,[3] Sophie Lambotte,[6] Frédéric Lauret,[1,4] Félix Léger,[1] Emmanuel Maros,[2] Aline Peltier,[1,4] Jérôme Vergne,[8] Claudio Satriano,[1] Frédéric Tronel,[7] Jérôme Van der Woerd,[6] Yves Fouquet,[2] Stephan J. Jorry,[2] Emmanuel Rinnert,[2] Isabelle Thinon[11] and Nathalie Feuillet[1]

[1] *Université de Paris, Institut de Physique du Globe de Paris, CNRS, F-*75005 *Paris, France. E-mail: saurel@ipgp.fr*
[2] *IFREMER, Centre de Bretagne, –Unité Géosciences Marines,* 1625 *Rte de Ste Anne,* 29280 *Plouzané, France*
[3] *BRGM, French Geological Survey, Risk and Prevention Division, F-* 45100 *Orléans, France*
[4] *Observatoire volcanologique du Piton de la Fournaise, Institut de Physique du Globe de Paris, F-*97418 *La Plaine des Cafres, La Réunion, France*
[5] *Université de La Réunion, Laboratoire GéoSciences Réunion, F-*97744 *Saint Denis, La Réunion, France*
[6] *ITES, Institut Terre Environnement de Strasbourg, UMR* 7063, *CNRS Université de Strasbourg,* 5, *rue René Descartes,* 67084 *Strasbourg, France*
[7] *BRGM, French Geological Survey, Regional Division (Mayotte), F-*97600 *Mamoudzou, Mayotte, France*
[8] *EOST, Université de Strasbourg/CNRS,* 5 *rue Descartes,* 67084 *Strasbourg Cedex, France*
[9] *Université Clermont Auvergne, CNRS, IRD, OPGC, Laboratoire Magmas et Volcans, F-*63000 *Clermont-Ferrand, France*
[10] *Istanbul Technical University, Faculty of Electrical and Electronics Engineering - Graduate School, Electronics and Communications Engineering Department, 34469 Maslak/Istanbul, Turkey*
[11] *BRGM, French Geological Survey, Georesources, F-*45100 *Orléans, France*

Accepted 2021 September 22. Received 2021 September 14; in original form 2021 February 24

SUMMARY

The brutal onset of seismicity offshore Mayotte island North of the Mozambique Channel, Indian Ocean, that occurred in May 2018 caught the population, authorities and scientific community off guard. Around 20 potentially felt earthquakes were recorded in the first 5 d, up to magnitude M_w 5.9. The scientific community had little pre-existing knowledge of the seismic activity in the region due to poor seismic network coverage. During 2018 and 2019, the MAYOBS/REVOSIMA seismology group was progressively built between four French research institutions to improve instrumentation and data sets to monitor what we know now as an on-going exceptional submarine basaltic eruption. After the addition of 3 medium-band stations on Mayotte island and 1 on Grande Glorieuse island in early 2019, the data recovered from the Ocean Bottom Seismometers were regularly processed by the group to improve the location of the earthquakes detected daily by the land network. We first built a new local 1-D velocity model and established specific data processing procedures. The local 1.66 low V_P/V_S ratio we estimated is compatible with a volcanic island context. We manually picked about

125 000 *P* and *S* phases on land and sea bottom stations to locate more than 5000 events between February 2019 and May 2020. The earthquakes outline two separate seismic clusters offshore that we named Proximal and Distal. The Proximal cluster, located 10 km offshore Mayotte eastern coastlines, is 20–50 km deep and has a cylindrical shape. The Distal cluster start 5 km to the east of the Proximal cluster and extends below Mayotte's new volcanic edifice, from 50 to 25 km depth. The two clusters appear seismically separated, however our data set is insufficient to firmly demonstrate this.

Key words: Indian Ocean; Volcano seismology; Volcano monitoring; Africa; Remote sensing of volcanoes.

1. INTRODUCTION

Before 10 May 2018, Mayotte island, part of the volcanic Comoros archipelago in the North Mozambique Channel of the Indian Ocean (Fig. 1), was not considered as a significantly seismically active area (Bertil & Regnoult 1998). The last reported widely felt earthquakes occurred around 30 km west of Mayotte: a moment magnitude (M_w) 5.0 event on 9 September 2011 (EMS98 intensity V estimated) and a magnitude (M) 5.2 event on 1 December 1993 (Lambert 1997) with moderate damages (EMS98 intensity VI estimated). Together with an unfelt M 5.1 event on 23 March 1993, 80 km southwest of Mayotte, these were the only $M5+$ earthquakes recorded within 100 km of the island since the advent of the global seismological networks in 1964 (Storchak *et al*. 2017; ISC 2020). As a consequence, only one real-time seismic station (RA.YTMZ; Résif 1995) was installed on the island at the onset of the 2018 seismic crisis. This station was deployed by BRGM (Bureau de recherches géologiques et minières, the French geological survey) for the French accelerometric monitoring network (Résif-RAP, Péquegnat *et al*. 2008).

On 10 May 2018, the first felt earthquake, quickly followed by many others, surprised inhabitants. More than 130 $M4+$ earthquakes were recorded in the following months, with the strongest being a M_w 5.9 on 15 May 2018 (GCMT project, Dziewonski *et al*. 1981; Ekström *et al*. 2012; Lemoine *et al*. 2020a). After about 50 d of very intense seismic activity, this unprecedented seismic sequence continued less intensively. During the summer of 2018, Global Navigation Satellite System (GNSS) data from the locally continuously recording sites began to show rapid surface displacements of the island (Briole 2018; Cesca *et al*. 2020; Lemoine *et al*. 2020a). Their elastic modelling evidence a large regional deflation centred east of Mayotte's shorelines (Cesca *et al*. 2020; Lemoine *et al*. 2020a). On 11 November 2018, a very low frequency tremor was recorded worldwide (Satriano *et al*. 2019; Cesca *et al*. 2020; Lemoine *et al*. 2020a), confirming that the seismic crisis was very likely of magmatic origin. This was later confirmed by the discovery of a new submarine volcanic edifice offshore Mayotte during the MAYOBS1 scientific expedition onboard *RV Marion Dufresne* in May 2019 (Feuillet *et al*. 2021). This large eruption began either on June 18 (Cesca *et al*. 2020) or on 3 July 2018 (Lemoine *et al*. 2020a).

Since the onset of the crisis, collaborations were progressively established between French research institutes to improve the understanding and knowledge of the on-going crisis. These collaborations enhanced the seismic monitoring of the region, which included installing additional real-time sites onshore, access to real-time data recorded by existing regional stations and offshore deployments. During the first year of the crisis, the monitoring network thus evolved rapidly (Lemoine *et al*. 2020a). In March 2019, 1 month after funding, four seismic stations were installed onshore (three on Mayotte island and one on Grande Glorieuse island) and six Ocean Bottom Seismometers (OBS) were deployed offshore, within a radius of 40 km around the seismically active area. A seismology team was created among the researchers, engineers, and students belonging to the participating French institutions (BRGM; Institut de Physique du Globe de Paris—IPGP; Institut Français de Recherche pour l'Exploitation de la Mer—IFREMER; Institut National des Sciences de l'Univers du Centre National de la Recherche Scientifique—INSU-CNRS). In July 2019, the Mayotte seismo-volcanic monitoring network (Réseau de surveillance volcanologique et sismologique de Mayotte—REVOSIMA) was created with all four institutions. The aim of the team is to process newly acquired data as quickly as possible and to obtain first hand results in almost real-time, to improve the daily monitoring and the knowledge of the volcano-seismic crisis.

In this paper, we review the local seismic network improvements since the beginning of the crisis and our scientific developments. We detail how this collaborative work was orchestrated for maximum efficiency and how it led to an improved local velocity model and a seismic catalogue from February 2019 up to May 2020 to better document the Mayotte 2018-ongoing seismo-volcanic crisis.

2. SEISMIC NETWORK EVOLUTION AND DATA PROCESSING

From May 2018 to June 2019, the Mayotte local real-time seismic network progressively evolved from 1 to 8 stations. Daily data analysis protocols have also been continuously adapted in several Institutes by our group to take advantage of the increasing number of local stations and to produce better locations for the detected events (see details in Section 2.2). In 2019, we also developed a new protocol to efficiently process OBSs data during pickathons, when, at the same place, several analysts dedicate a few days to work together on the newly recovered data.

2.1 Development of the monitoring network

2.1.1 The in-land network

At the beginning of the seismic crisis, Mayotte's seismicity was monitored by the BRGM with the only local real-time seismic station from the French Résif-RAP accelerometric RA network (YTMZ; Résif 1995) and some regional stations from international networks (IRIS/IDA, GEOFON and GEOSCOPE in Madagascar, Kenya, Seychelles and La Réunion). In the Comoros archipelago, the Observatoire Volcanologique du Karthala (OVK) monitors the Karthala volcano (Grande Comore) since 1988. The OVK seismic network, while located 250 km northwest from Mayotte (Fig. 1b), was crucial for characterizing Mayotte's seismicity, particularly at

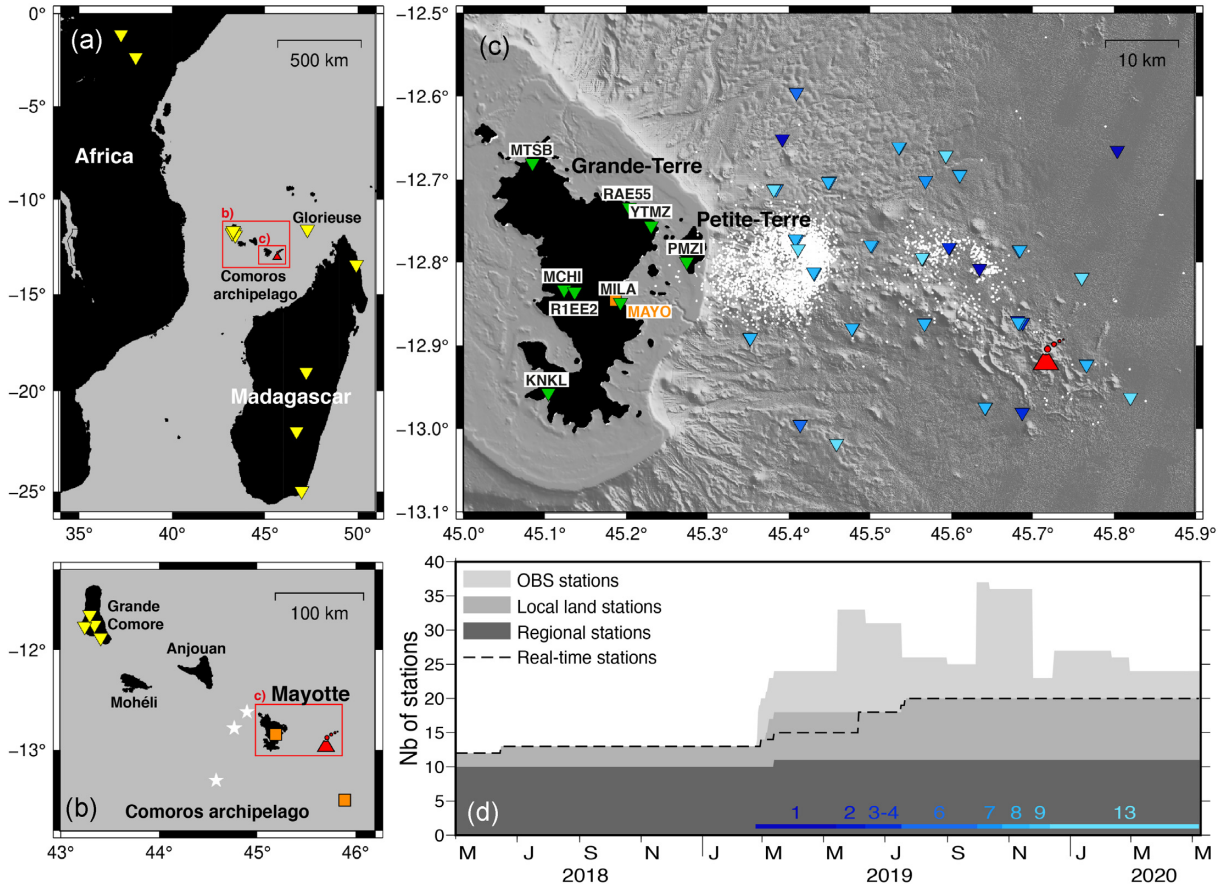

Figure 1. Maps of seismological land stations and Ocean Bottom Seismometers (OBSs) used in this study with the red volcano symbol representing the location of the new volcanic edifice (Feuillet *et al.* 2021). (a) Map showing the regional stations contributing to the monitoring (yellow inverted triangles). Red rectangles highlights the Comoros archipelago area shown in (b) and the Mayotte area shown in (c). (b) Map of the Comoros archipelago showing the temporary stations used for previously-developed velocity profiles (orange squares), historical $M > 5{,}0$ earthquakes close to Mayotte (white stars) and the Karthala seismic network (yellow inverted triangles). (c) Map of the local land stations (green inverted triangles, most of them installed in 2019) and all OBSs deployed between February 2019 and May 2020 [blue inverted triangles, the blue hue depends on the MAYOBS deployment timing as seen in (d)]. The MAYO station (orange square) is the temporary station used by Dofal *et al.* (2018) receiver function study. The white dots represent the 5000 manually relocated earthquakes. (d) Time evolution of the number of recording stations since the onset of the crisis. All regional stations (dark grey) are available in real-time. Local stations (added to the regional stations; in grey)—significantly increased in number in 2019. The number of OBSs (added to the local and regional stations; in light grey) varies over time depending on the MAYOBS deployment period (blue scale on bottom right numerated as the MAYOBS oceanographic campaigns that recovered them). The dashed line represents the evolution in time of the number of real-time stations.

the beginning of the sequence. Real-time seismic data recorded at Karthala volcano were shared during the first weeks of the crisis via its French partner in the Indian Ocean, the Observatoire Volcanologique du Piton de la Fournaise (OVPF-IPGP). In June 2018, a medium-band station was installed at a Mayotte school (ED.MCHI), cofunded by the local representation of the ministries of environment (DEAL) and of education as well as the BRGM, within the program *Edusismo* (Virieux 2000). By the end of June 2018, the seismicity decreased after one and a half month of intense activity. At that time, the BCSF-RéNaSS (Bureau Central Sismologique Français—Réseau National de Surveillance Sismique), in charge of the macroseismic and intensity investigations on the national territory, performed a macroseismic field survey on Mayotte (Sira *et al.* 2018) and took advantage of this mission to install two RaspberryShake instruments (Bès de Berc *et al.* 2019) from the AM network (Raspberry Shake Community *et al.* 2016): RAE55 and RCBF0. RCBF0 station unfortunately failed after 2 weeks. The local onshore network (Fig. 1) was not upgraded again until March 2019 with the installation of three stations: two Guralp CMG40T medium-band sensors from the 1T temporary network (Feuillet, Van der Woerd and RESIF, 2022)—MTSB and PMZI; and one Nanometrics Trilium120PA broad-band sensor from the QM network—KNKL. Safety and rapid deployment on a small island, as well as network geometry, were key criteria to choose the station sites. The stations were therefore installed in city halls or public buildings to ensure a stable power supply and protection from theft. In the same time, a seismic station with triggered data transmission from the QM network (GGLO) was installed on Grande Glorieuse, a small island 250 km northeast from Mayotte, completing the regional network in March 2019. Finally, two RaspberryShake instruments were added to the AM network by RéNaSS in June 2019 on Mayotte: R1EE2 and R0CC5 (colocated with RA.YTMZ station).

2.1.2 The OBS network

At the end of February 2019, six short-period OBSs from the INSU-IPGP OBS facility were deployed from a barge around the

earthquake locations that were known at the time (Bertil *et al*. 2019). The INSU-IPGP OBSs are free-fall instruments with 1-yr maximum autonomy, whose sensors are a 3-channel geophone and a broad-band hydrophone. There have been several recoveries and redeployments of OBSs since then, but there have always been 4–16 OBSs deployed (Fig. 1d), which have greatly improved the azimuthal coverage of the local seismic network, as will be discussed later in the paper. The INSU-IPGP OBSs were regularly complemented with IFREMER micrOBSs or LotOBSs, hosting a similar geophone and a short-period hydrophone but with an autonomy, respectively, limited to 45 or 120 d maximum. After the initial deployment, area specific location protocol establishment and much more precise location of the seismicity, the OBS network geometry remained stable and a number of positions were re-occupied during subsequent deployments (Figs 1c and d).

Data acquisition protocol differs depending on the instruments—land or ocean-bottom based. Data from land stations are acquired and transferred in real-time, except the regional QM.GGLO station from which only triggered data can be transmitted via a low-bandwidth satellite link. The onshore data are centralized at the IPGP data centre and then made available through the same protocol on its public SeedLink server. The three stations installed on Mayotte in March 2019 were not equipped with internet connection during the first months of recording but were brought online in May 2019. Their data were manually collected from the internal storage just before the departure of the *RV Marion Dufresne* for the MAYOBS1 oceanographic campaign in May 2019 (Feuillet 2019).

The OBSs are regularly serviced for maintenance and data recovery (every 3–4 months for INSU-IPGP, every month for micrOBSs). As of May 2020, nine different OBSs deployments have been conducted. When the OBSs are recovered, their data are downloaded and time-corrected for internal clock drift and converted to miniSEED format using L-Cheapo tools (Orcutt & Constable 1996). These data are then integrated in the main waveform database at the IPGP data centre, along with the local and regional land station data.

2.2 Data analysis

2.2.1 Daily monitoring

For daily monitoring of the crisis, only the real-time data from land stations can be used. Several institutes successively participated in the day-to-day seismic data processing, using SeisComP3 (Weber *et al*. 2007) with slightly different setups. The BRGM office in Mayotte was involved first and maintained a seismic catalogue from the beginning of the crisis in May 2018 (Bertil *et al*. 2018, 2019). The events from Bertil *et al*. (2018, 2019) were located from manually picked waveforms using the LocSAT algorithm (Bratt & Bache 1988) and a slightly modified IASPEI91 velocity model (Kennett & Engdahl 1991). During the summer of 2019, with the addition of new local stations available in real-time, the RéNaSS hosted by the Ecole et Observatoire des Sciences de la Terre in Strasbourg (EOST) improved the settings of its SeisComP3 automatic detection system by using STA/LTA automatic picking and grid-search location. They took over the role of manually picking all automatically detected events for the newly created Réseau de surveillance Volcanologique et Sismologique de Mayotte (REVOSIMA) working group. The RéNaSS also used LocSAT but with the original IASPEI91 model. In April 2020, the daily manual picking and location duty was transferred to OVPF-IPGP in La Réunion, which uses the NonLinLoc (NLL) location software (Lomax *et al*. 2014) and a new hybrid velocity model described in Section 3. The NLL configuration and 1-D local velocity model used by OVPF-IPGP in La Réunion were developed during MAYOBS1 campaign in 2019 (Feuillet *et al*. 2019; Saurel *et al*. 2019; Feuillet 2019).

While a daily manual screening of continuous waveforms with WebObs (Beauducel *et al.* 2020) and identification of every event has been performed since early 2019, the composite earthquake catalogue is based on the automatic detection of events from land stations. The land stations influence the magnitude detection threshold for two reasons. First, the land-based seismic network has evolved since May 2018, and second, the chosen sites that offered equipment safety are often affected by anthropogenic noise, implying a daily variation of the magnitude detection threshold. Since the drastic improvement of the local land network in spring 2019, the detection threshold is around $M2.0$ at nighttime and around $M2.5$ during daytime.

2.2.2 OBS integration

After each OBSs data recovery, we manually pick phases on the OBS data and offline land stations to improve the locations in the existing earthquake catalogue during dedicated pickathons that continue today. Adding new phase picks significantly improved the location of the earthquakes already detected and first located only by the land network. Since there are already a great number of events to relocate in the existing catalogue, we do not search for new events from the OBS data set. Searching for new events in the OBS data set is a work in progress and will be reported in future studies. During each pickathon, the time span of the OBSs data we need to process is divided across three teams using the same software setup and each team manually locates earthquakes in descending order of magnitude (Saurel *et al*. 2019; Fig. 2). When the OBSs are recovered from an oceanographic research vessel, such as *RV Marion Dufresne*, large enough to board a team of around 10 analysts, we divided the work in three 4-hr-shifts (i.e. 2 or 3 analysts by shift) we can manually pick earthquakes 24/7. Otherwise, the MAYOBS/REVOSIMA seismology group meet—either virtually or at one of the group institutes—for 2 d to process the recently recovered data, produce graphics demonstrating the evolution of the crisis, and interpret the results together. Whether the phase picking, location, and interpretation are done onboard or on land, we use the same setup/configuration, starting database, and software to analyse the recently recovered data. We assigned uncertainty to each phase, from a common predefined list of values. Time uncertainties assigned to the S-phase were always equal to or larger than the uncertainty assigned to the *P*-phase. Impulsive *P*-phase polarity onset is also reported for first motion source mechanisms studies later use. We were able to locate events as small as M 0.8, but despite improvement since July 2019 and the use of more stations in the STA/LTA automatic processing, their detection is far from complete and mainly depends on the land station daily noise level. We estimate that the magnitude of completeness is below M 3.0 (see Section 4) whatever the time allocated to the processing during each pickathon and the number of events processed. We typically process around 1000 earthquakes during pickathons when performed onboard scientific cruises and around 500 earthquakes during pickathons conducted on land. So far, our catalogue contains more than 5000 manually picked earthquakes from February 2019 to May 2020, relocated using combined land and OBS data.

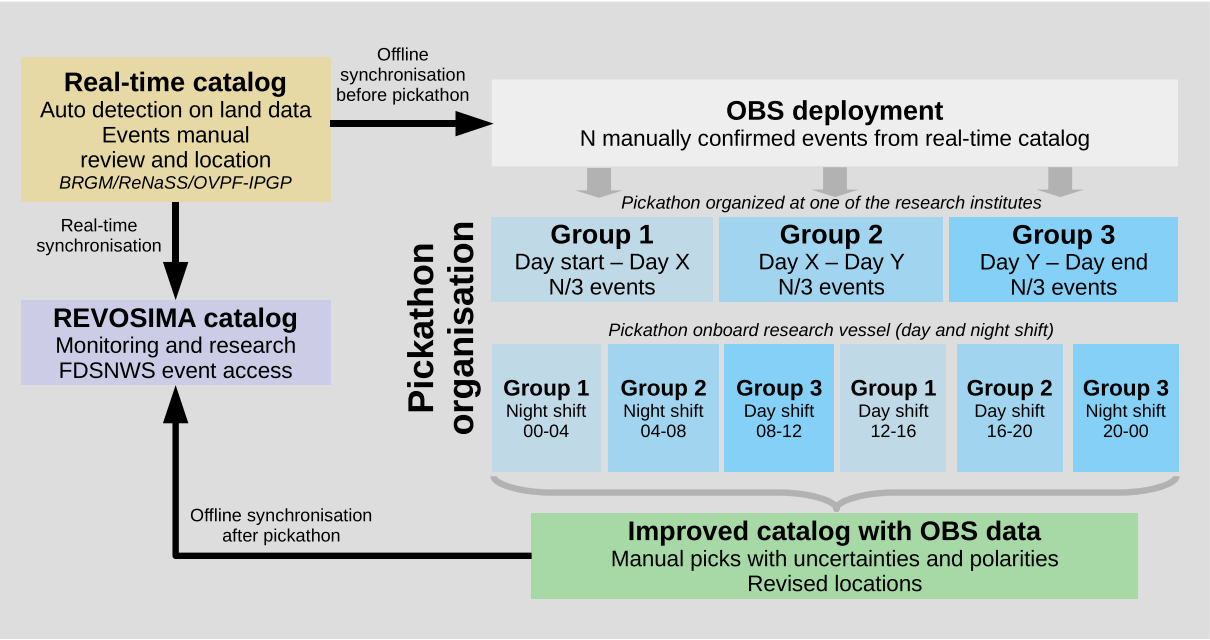

Figure 2. Typical pickathon organization. After each OBS recovery, the deployment time-span is divided in three groups, that is Group 1, Group 2 and Group 3. Each group processes the same number of events, by decreasing magnitude order, using the same software setup and the same picking guidelines and recommendations. The daily catalogue of events, automatically detected and manually confirmed on land-based network data (BRGM then RéNaSS and OVPF-IPGP), is synchronized in the pickathon database. It also feeds in real-time the REVOSIMA/MAYOBS catalogue. When OBS recovery is performed by a research vessel, each group alternates a 4-hr day and night shift. At the end of the pickathon, the relocated events, with additional manual picks and polarities on OBSs data, is merged within the REVOSIMA/MAYOBS database for further use for monitoring and research. The same procedure is applied to on land pickathons, only the work is completed during 2.5 normal work days instead of 24-hr shifts.

To enable this collaborative work, we use techniques and configurations developed during the last 10 yr for the daily routine processing of earthquakes in IPGP volcanic and seismologic observatories. Waveform data and event databases are held by a SeisComP3 instance (Weber *et al*. 2007). Each earthquake analyst uses their own laptop and, regardless of their laptop's Operating System, they run a VirtualBox pre-configured Linux machine with the SeisComP3 Origin Locator GUI client (scolv, Weber *et al*. 2007). We use NLL software and the new local 1-D velocity model described in the following section to locate the events. Magnitudes are computed with the embedded local magnitude (M_L) formula in SeisComP3 (Richter 1958). The horizontal signals are converted to a Wood-Anderson seismometer response (Urhammer & Collins 1990) before measuring their pick amplitude. We have not yet calibrated this magnitude as very few of the earthquakes since 2019 have been characterized with a moment tensor magnitude by the global monitoring agencies (GCMT project, Dziewonski *et al*. 1981; Ekström *et al*. 2012).

3. IMPROVED 1-D LOCAL VELOCITY MODEL

A local velocity model is essential to provide precise location of this dense swarm seismicity. One of the first challenges in improving earthquake locations was then to build a reasonable 1-D local velocity model, because only global models were available so far. This was done onboard *RV Marion Dufresne* during the MAYOBS1 campaign (Feuillet 2019). We used the data of the first OBSs recovery and of three local land stations (see Section 2). We first produced modified Wadati diagrams (Chatelain 1978) and considered two different existing velocity profiles from the area. The first profile, named 'Coffin449', is based on a *P*-wave velocity (V_P) profile derived from a 1980 active-seismic sonobuoy. That experiment was located 100 km southeast of Mayotte (Coffin *et al*. 1986, instrument 449; Fig. 1b) and extended beyond 10 km depth with a Moho interface 15 km deep (Jacques *et al*. 2019). The second profile, named 'ADofal', is based on a *S*-wave velocity (V_S) profile determined from receiver functions (Dofal *et al*. 2018) using the MAYO temporary station deployed on Mayotte island between 2011 and 2014 (RHUM-RUM project, doi:10.15778/RESIF.YV2011; Fig. 1b). After adding phases from OBSs to 100 events during an onboard pickathon, we located them with Hypo71 (Lee & Lahr 1972) and the 'Coffin449' model with a V_P/V_S ratio of 1.80 extrapolated from Eastern and Central Afar studies (Jacques *et al*. 1999; Grandin *et al*. 2011). The modified Wadati diagrams (Chatelain 1978) indicated a local (OBS and Mayotte land stations) V_P/V_S ratio of 1.66 and a regional V_P/V_S ratio of 1.72 (Figs 3a and b).

We then tested different combinations of velocity model parameters (2 velocity profiles and 3 V_P/V_S ratios) on a more complete data set of 800 events with OBS phases, using NLL software (Lomax *et al*. 2014). Contrary to Hypo71, NLL allows the use of depth variations of the V_P/V_S ratios and different velocity models depending on the station. Its probabilistic approach (Lomax *et al*. 2014) also makes the reported ellipsoidal errors more meaningful and easier to interpret than estimated horizontal and vertical errors given by Hypo71. We first used only local stations (Mayotte land stations and OBSs) arrivals to assess the best local 1-D velocity model. We compared the distributions of maximum ellipsoidal error for the 2 velocity models and 3 V_P/V_S ratios for the 800-earthquakes MAYOBS1 data set. The ellipsoidal error major axis ranges between 2 and 10 km, with most of the events at 4 $\pm$ 2 km. The

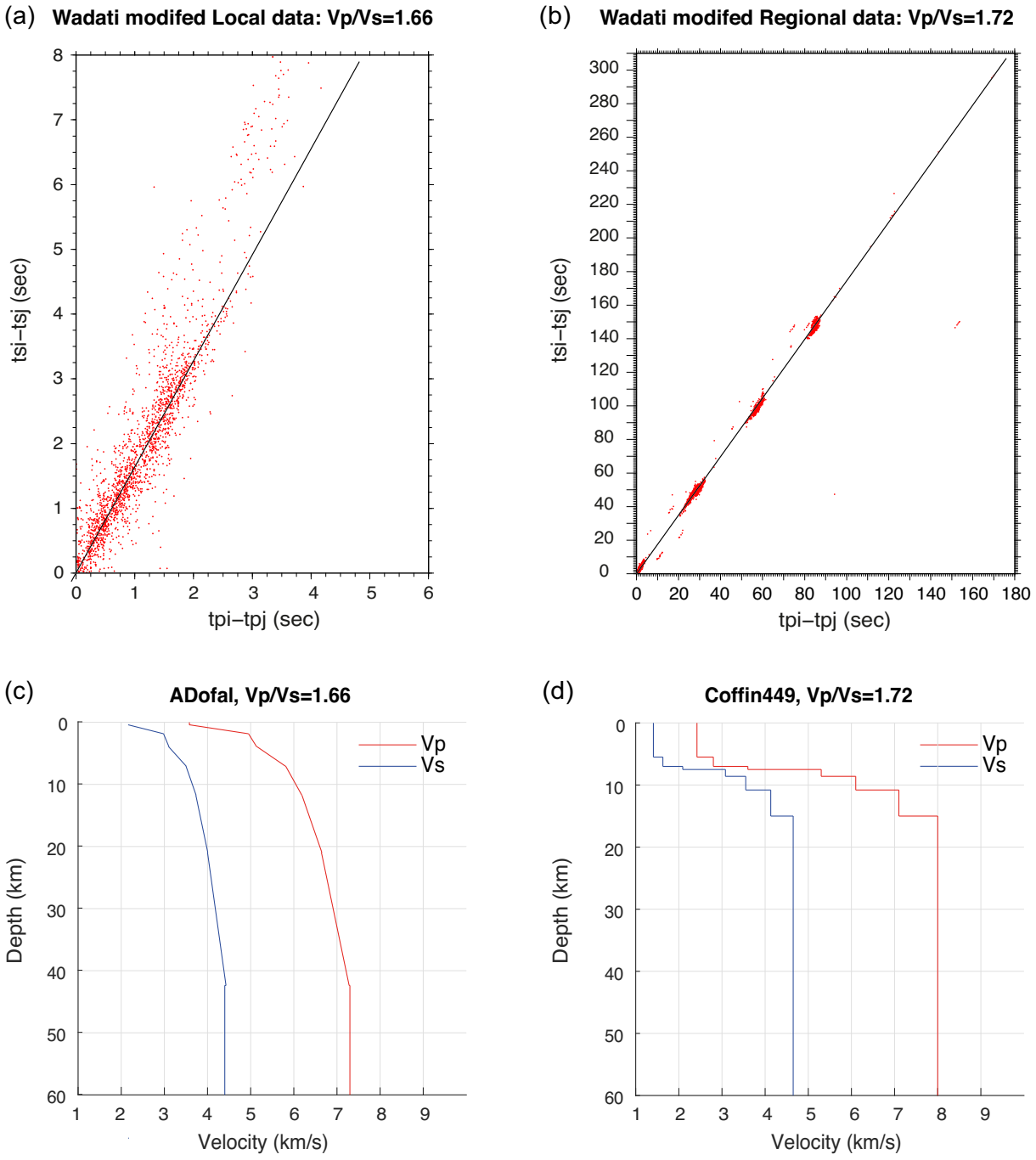

Figure 3. Modified Wadati diagram of *P* and *S* waves arrival times for the first hundred OBSs+ land relocated earthquakes. Differences in *S*-wave arrival times (tsi, tsj) are plotted against differences in *P*-wave arrival times (tpi, tpj) for station pairs(i,j). (a) Plot for local stations only (Mayotte land stations and OBSs): $V_P/V_S = 1.66$. (b) Plot for local and regional stations: $V_P/V_S = 1.72$. (c) ADofal gradient velocity model with V_S from a Mayotte station receiver function and 1.66 V_P/V_S ratio used for Mayotte land stations and OBSs. (d) Coffin449 velocity model with V_P velocity profile from sonobuoy experiment and 1.72 V_P/V_S ratio, used for regional stations (Comoros archipelago and Grande Glorieuse).

best results (low average value and limited spreading of the ellipsoidal errors) were obtained using the 'ADofal' velocity model with $V_P/V_S = 1.66$, for which 83.5 per cent of the events had maximum ellipsoidal errors smaller than 5 km. The 'Coffin449' model was a better match for the closest regional station arrivals (Comoros and Grande Glorieuse), with $V_P/V_S = 1.72$. The AK135 velocity model (variable V_P/V_S, Kennet *et al.* 1995) in combination with 'ADofal' and 'Coffin449' gave lower residuals on global station arrivals (Africa, Madagascar and Indian Ocean) than the IASPEI91 model. Our final velocity model is a hybrid model (see Tables S1, S2 and S3 for layered detailed values) composed of: the 'ADofal' model with $V_P/V_S = 1.66$ (Fig. 3c) for OBSs and stations on Mayotte; the 'Coffin449' oceanic model with $V_P/V_S = 1.72$ (Fig. 3d) for regional stations (between 200 and 400 km from Mayotte) and the AK135 global velocity model for more distant stations. NLL also computes a V_P/V_S ratio for each event, based on *P*- and *S*-arrival times and

independent from earthquake location, using a formula described in the HypoEllipse manual (Lahr 2012). The NLL estimation, using the 800 events, supports the mean V_P/V_S ratios previously estimated for local and regional stations on the first 100 events.

With this new hybrid 1-D velocity model, the earthquake lie between 25 and 55 km depth (Figs 4a–c). They are in the mantle, below the Moho discontinuity, which has been estimated either at 17 km depth under Mayotte island by Dofal *et al*. (2018) or at 15 km depth offshore by Jacques *et al*. (2019). This is very unusual compared to other volcanoes where deep seismicity is usually sparse and of low energy (White & McCausland 2019). To confirm our earthquake locations, we performed further robustness tests of our hybrid 1-D velocity model to exclude any potential depth bias, for example a soft-sediments layer impacting *S*-wave arrivals as has been influential along a segment of the SW Indian Ridge (Grevemeyer *et al*. 2019). The earthquake depth distribution remains stable whatever the velocity models and V_P/V_S ratios we tested (Figs 4a and b). Only one model, the 'Coffin449' oceanic crust-like model, with an unrealistic V_P/V_S ratio of 1.8 (with regards to the observed ratios from arrivals time data), gives significantly shallower depths, between 10 and 40 km (Fig. 4b, red dashed line). In this case, the mean time residual RMS increases from less than 0.2 s for all 5 other velocity models to 0.3 s. We then compared the depth distribution of a high-quality subset of the MAYOBS1 catalogue, that is 149 earthquakes with at least 5 *P*-wave and 5+-wave arrivals picked on the OBSs data, using different altered configurations and velocity models. Removing *S*-arrivals or adding a 0.2 km s^{-1} *S*-wave slow velocity, 200-m-thick sediment layer—consistent with soft unconsolidated sediments—does not change significantly the depth range of events (Fig. 4c). The mean time residual RMS however reaches 0.34 s with the sediment layer, compared to 0.24 s with our model. We can conclude that the addition of a reasonably dimensioned superficial unconsolidated sediment layer would thus only have a small effect on the depth distribution, compared to the use of our velocity model. Using *P* arrivals only confirms that there is no *S* arrivals related bias in our velocity model. Finally, we used both *P* and *S* arrivals in uniform half-space velocity models with our 1.66 V_P/V_S ratio (Fig. 4d). For a reasonable half-space *P*-wave velocity between 5 and 9 km s^{-1}, all events are located between 20 and 60 km depth, with an average RMS lower than 1 s and best results obtained with $V_P = 6$ km s^{-1}. Except in the extreme cases, earthquakes were always located deeper than 15 km (Jacques *et al*. 2019).

4. EARTHQUAKES LOCATIONS

The REVOSIMA reported 30 000 events between 25 February 2019 and 10 May 2020, based on manual screening of the continuous land data. Using NLL software and our new 1-D hybrid velocity model within SeisComP3, we located more than 5000 of those events, which have already been detected from the land stations (Fig. 5; Saurel *et al*. 2021). The mean absolute location accuracy is around 2 km vertically (Fig. 5a) and 2.5 km horizontally (Fig. 5b). The formal horizontal and vertical uncertainties are both lower than 5 km with an azimuthal gap less than 175° (Fig. 5c) for 95 per cent of all earthquakes. The location accuracy does not show much variations with the different OBS network geometries and the number of OBSs used for location (Fig. 5d). That is to say, the OBSs network is always sufficient to reduce the azimuthal gap to less than 175° and to increase the number of phase arrivals used for location to more than 15 phases. Because we processed the data in descending magnitude order, we always achieved a magnitude of completeness of 3.0 or lower (Fig. 5e). At present, we now have a data set of nearly 125 000 manual *P* and *S* phases between February 2019 and May 2020 (Fig. 5f).

This relocated earthquake data set, while only comprising a part of the recorded seismicity allows us to identify two distinct seismically active zones (Fig. 6a).

The Proximal cluster, with 90 per cent of the located earthquakes, is situated close to the Mayotte island of Petite-Terre. In map view, it has a circular shape (Fig. 6c) and spans depths ranging 20–50 km (Fig. 6b). Most of the seismicity is concentrated on the eastern side of the circle, where the highest magnitudes are located (all *M*4–*M*5+ events of the cluster). On the western side of the circle, closer to Mayotte's coasts, the events magnitudes are lower, and the seismicity is more diffuse. At depth, 2 different patches can be identified (Fig. 6d): one patch is dipping towards Petite-Terre, with events located between 35 and 45 km depth and a second patch is more vertical, with events located between 25 and 40 km depth. The north–south thin (2 km wide) cross-section (Fig. 6e) also shows 2 subvertical lines of earthquakes, suggesting a cylindrical cluster with a lower earthquake density in the centre (Fig. S3). Based on the earthquake density, we can estimate an outer diameter of 11 km, and an inner diameter of 3 km.

The distal cluster is located just a few kilometers to the east of the Proximal cluster, and contains earthquakes with depths ranging between 25 and 50 km (Fig. 6g). It is not seismically connected to the Proximal cluster in our data set. Its seismicity is spread on a N130°E trend extending towards the new volcano edifice (NVE). Earthquakes along its northwest part are concentrated between 35 and 50 km depth. This area concentrates most of the highest magnitudes events located in the distal cluster. The depths of the shallowest earthquakes progressively decrease up to 25 km (Fig. 6g) as they approach the NVE. Because our velocity model was built during the MAYOBS1 cruise, during which we still had intense seismicity with most of the highest magnitude earthquakes of our data set that occurred in the Proximal cluster (Feuillet *et al*. 2021), only a few events were located in the Distal cluster. Our velocity model is then mostly constrained by the Proximal events. This may explain why the seismicity close to the NVE seems less clustered and more loosely located.

We did not locate any earthquake with reliable depths shallower than 20 km during the period of investigation (Fig. 6d). However, because we only relocated events that have already been automatically detected and located using only the land stations network, we might have missed some shallow, local and low magnitude earthquakes.

5. DISCUSSION AND CONCLUSIONS

Thanks to the collaborations among several research institutions, we, the MAYOBS/REVOSIMA seismology team, has facilitated the deployment of multiple seismometers, as well as the collection and interpretation of their data since early 2019. The numerous pickathons we have held since then have improved our understanding of the seismicity occurring offshore Mayotte. The seismicity manually-picked and relocated in this study, from February 2019 to May 2020 is in agreement with the analysis of 2018 activity (Cesca *et al*. 2020; Lemoine *et al*. 2020a; Table 1), as seismicity clusters identified in this work seems to have been active since summer 2018. The Distal cluster correlates with the first cluster of activity that represents rock fracturing and dyke opening from the centre of deflation towards the volcano, leading to the creation of the NVE (Cesca *et al*. 2020; Lemoine *et al*. 2020a; Feuillet *et al*.

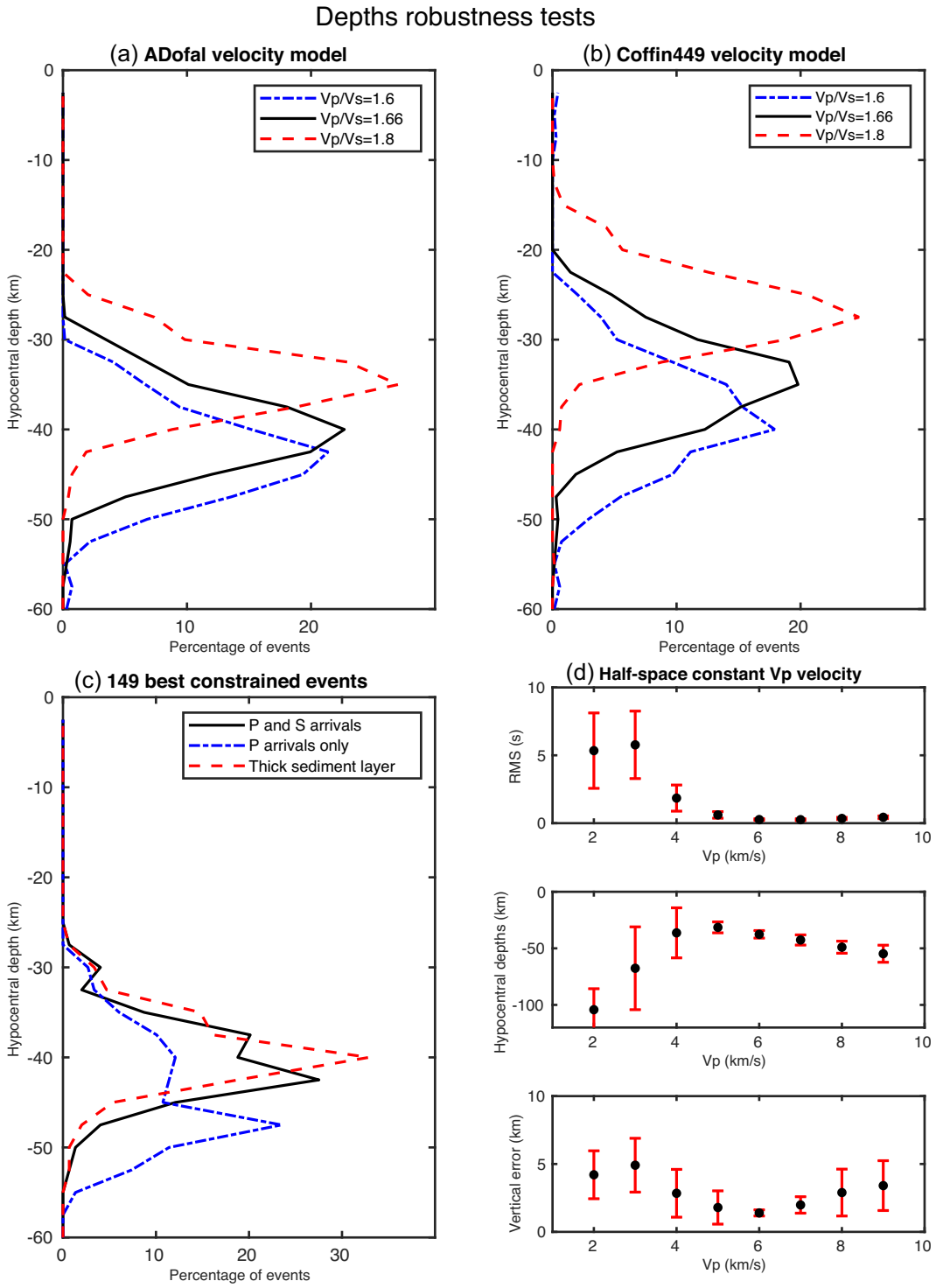

Figure 4. Depth robustness test results. (a) Distribution of the hypocentral depths of the OBSs+ land catalogue for ADofal *S*-velocity model and the different tested V_P/V_S ratios. (b) Distribution of the hypocentral depths of the OBSs+ land catalogue for Coffin449 *P*-velocity model and the different tested V_P/V_S ratios. (c) Depth distribution changes when adding an unconsolidated sediment layer below the OBSs (200-m-thick sediment layer with low *S*-wave velocity of 0.2 km s^{-1} below each OBS—dashed red) and when using *P* arrivals only (dotted–dashed blue). (d) Mean and standard variation of the RMS, depth and vertical error distributions for various *P*-wave velocity speeds and this study's V_P/V_S ratio of 1.66 using a homogeneous half-space velocity model. All tests were performed using NLL software.

2021). However, a notable difference with our catalogue is the lack of earthquakes in the first 20 km below the volcano. This could be explained by a magma path towards the surface now opened and generating only very small events not detected by the land network while the path fracturing the crust in 2018 implied strong felt earthquakes (Duputel *et al*. 2019). The Proximal cluster correlates with seismic activity that initiated during July 2018 (Cesca *et al*. 2020; Lemoine *et al*. 2020a) and became very active at the end of August

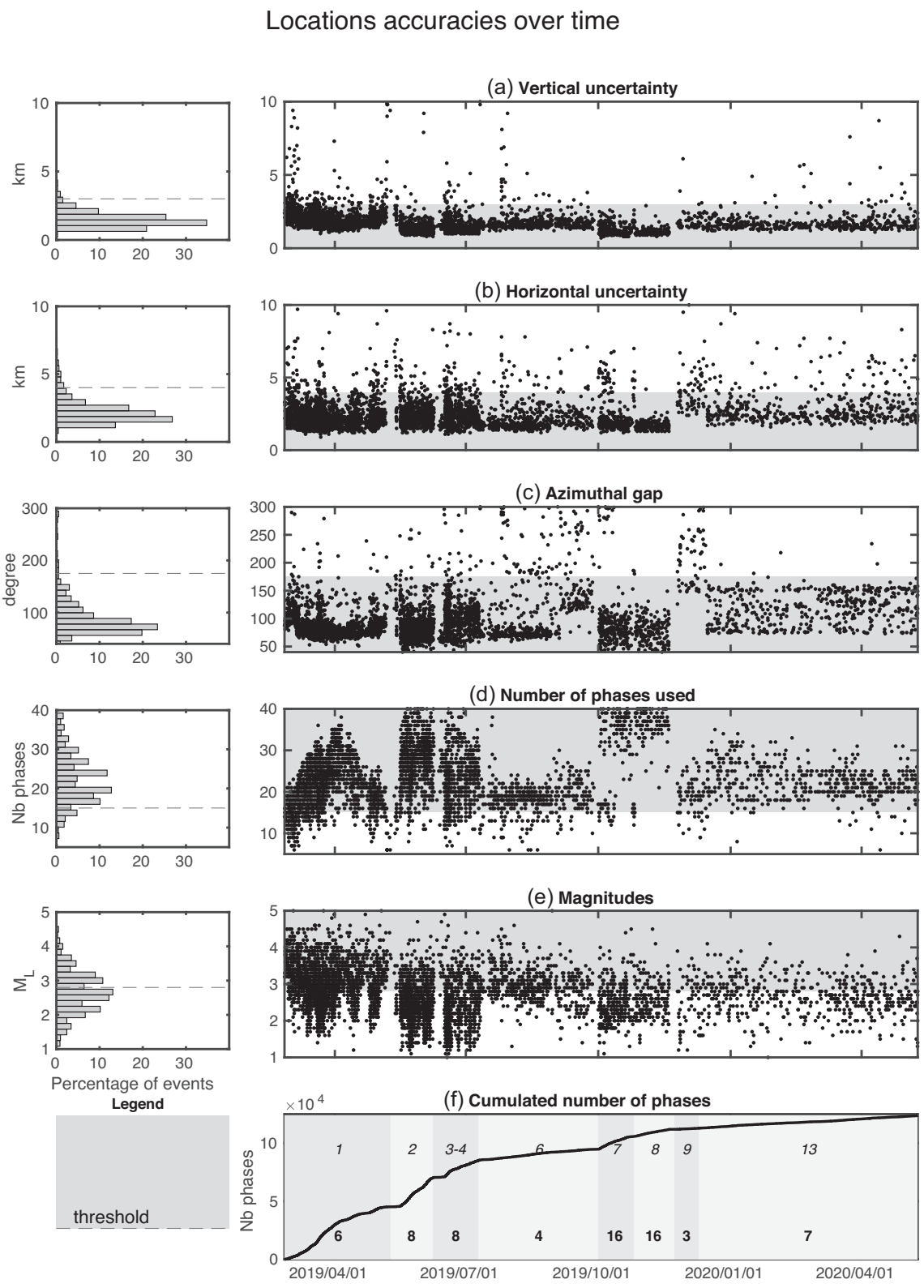

Figure 5. Distributions (left-hand panels) and time evolution (right-hand panels) for the 5174 earthquakes manually picked and relocated with OBSs data between 25 February 2019 and 10 May 2020, processed during the pickathons. The dashed line on each graph represents the minimum or maximum threshold reach for all the data set as described in this study. (a) Vertical uncertainties, mostly below 3 km. (b) Horizontal uncertainties, mostly below 4 km. (c) Azimuthal gaps, mostly below 175°. (d) The number of *P*- and *S*-wave phases used for each event, mostly above 15. (e) The local magnitudes of all events, with maximum magnitude of completeness at approximately 2.80. (f) The cumulative number of manual phases picked over time. Light and dark grey bands represent the different OBSs deployments over time. Italic numbers are the deployment IDs and relates to Fig. 1(d) indication. Bold numbers are the number of OBS instruments used for each deployment. Four denser deployments of 8 and 16 OBSs (including IFREMER micrOBS instruments) allows to significantly reduce the azimuthal gap. There are small gaps in the catalogue, which are due to the few days necessary to maintain and redeploy the OBS.

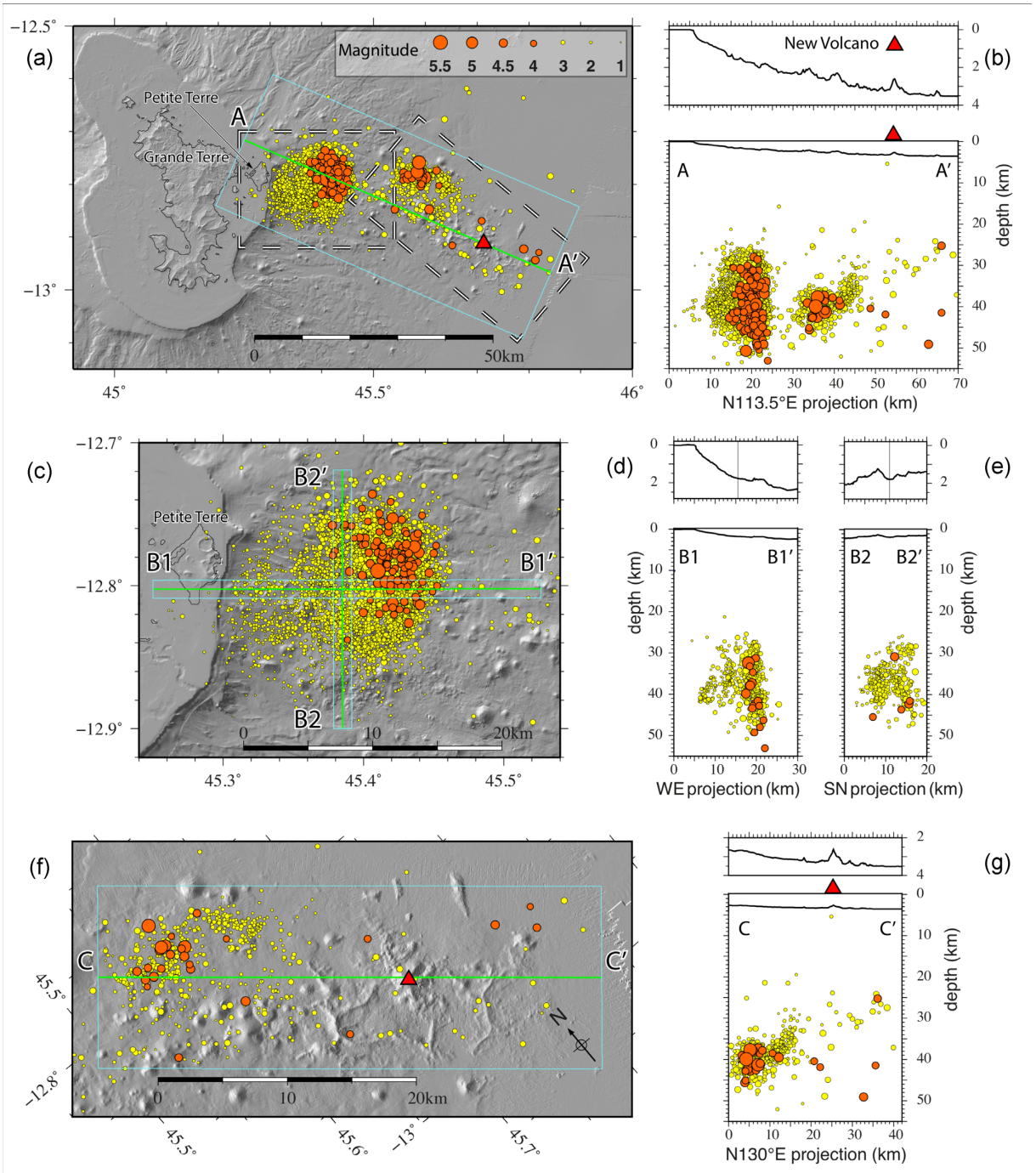

Figure 6. Earthquake location distributions. (a) Map of Mayotte earthquakes from 25 February 2019 to 10 May 2020 located using OBS data and (b) their distribution along a N113°E cross-section: the two active seismic clusters are seemingly disconnected. (c) Proximal cluster zoom showing its round shape and (d) 2-km-wide east/west cross-section and (e) 2-km-wide north/south cross-section suggesting a tube-like shape with subvertical alignments. More seismicity is visible in the eastern part of the cluster where there are all the $M > 4.0$ earthquakes (orange). The more diffuse seismicity on the west side is limited between 35 and 40 km depth within a vertical alignment dipping towards Mayotte island. (f) Distal cluster zoom showing the alignment of seismicity along a N130°E direction towards the NVE and (g) the N130°E cross-section showing seismicity depth variation. Thick dashed black boxes: locations of the Proximal and Distal cluster zooms; thin blue boxes: earthquake selection for the three cross-sections; green lines: associated topographic profiles; red triangles: location of the new volcanic edifice.

Table 1. Comparison of cluster names from this study (Cesca *et al.* 2020; Lemoine *et al.* 2020a), and REVOSIMA monthly bulletins.

This study	Lemoine *et al.* (2020a)	Cesca *et al.* (2020)	REVOSIMA monthly bulletins, 2019–2020
Distal cluster	Cluster 1 and Cluster 2	Dyke volcano-tectonic (VT, blue, cyan, purple)	Secondary
Proximal cluster	Cluster 3	Sagging volcano-tectonic (VT, red, green)	Primary

2018. This correspond to the beginning of the island subsidence and eastward displacement as recorded in GNSS data, inferred to be due to the drainage of an at least 30 km deep magma chamber (Briole 2018; Cesca *et al*. 2020; Lemoine *et al*. 2020a; Feuillet *et al*. 2021). This proximal cluster appears not connected to the Distal cluster in our data set and this seems to have been the case since the beginning of the crisis. The Proximal cluster cylindrical shape match existing interpretations of a slowly sagging caldeira piston (Cesca *et al*. 2020; Feuillet *et al*. 2021), but it could also be an ancient fault zone re-activated by the massive changes in lithosphere constraints due to the eruption. Further detailed interpretation of the Proximal cluster seismic activity requires results from ongoing studies (lithosphere structure studies, high-resolution relocations, source mechanisms).

The 2 local and regional velocity models used in this study with their respective V_P/V_S ratios are consistent with the two main geological setting interpretations of the area. The 'Coffin449' model upper low velocity layer and rapid increase up to a Moho at 15 km depth is compatible with an oceanic crust. Its averaged V_P/V_S ratio can explain an oceanic crust or mixed oceanic and continental crust at regional scale. The 'ADofal' model smooth velocity changes and the low local V_P/V_S ratios can be associated with an heterogenous volcanic island context: hot material and presence of gas or fluid-filled fractured rock. This low V_P/V_S ratio is also consistent with the *H–k* stacking from receiver functions performed by Dofal *et al.* (2021) and could support their interpretation of a continental crust with underplating similar to the magmatic continental domain of the southeastern coast of Madagascar (Rindraharisaona *et al*. 2017).

In terms of monitoring, the regular recovery and deployment of OBSs and the subsequent and immediate data analysis have been essential to monitor the Mayotte sismo-volcanic crisis. The wide collaboration between many scientists, engineers, and students, from different institutes and universities, during the pickathons continues to bolster rapid earthquake processing and has also fostered discussions on the evolution of the seismicity with the most up-to-date data. The magnitudes distribution over time (Fig. 5e) show that the seismic activity seems to have decreased in 2019, until October 2019 since when the magnitudes distribution is stable. This evolution can then be compared with the bathymetry surveys indicating the eruption is still ongoing at lower emission rates (REVOSIMA 2019). Onboard the monitoring cruises, information from this rapid processing is used to prioritize operations (bathymetry survey) and focus on the areas of interest and/or crisis. With each pickathon, we progressively increased our knowledge of the area, which in turn also feeds the hazard and risk assessment studies that will help the authorities with the decision-making process. For example, the Proximal cluster, while it does not seem directly linked to the magma emission at the new volcano is of particular concern since it is much closer to the island and even slightly expands below Mayotte. Tsunami modeling studies (Lemoine *et al.* 2020b; Poulain *et al.* 2021), up to impact mapping, were conducted with tsunamigenic sources derived from this improved knowledge of the seismicity.

The resulting high-quality data set of manually picked arrivals is now used in several detailed on-going studies (lithosphere structure investigations, seismicity time and space evolution, seismic sources studies, high-resolution locations) that will better constrain the seismicity, active structures and geological setting of the area. Various non-earthquake signals, such as hydro-acoustic or seismic waves not clearly associated to earthquakes, have been discovered during routine data screening and are currently being investigated. While REVOSIMA has reported more than 30 000 events for the period covered by the catalogue after daily manual screening of the continuous land stations data, our refined 5000 earthquake locations and 1-D velocity model ascertained by using OBSs data provides a solid foundation for future studies. Our anticipation is that our improved earthquake location catalogue, coupled with geodetic modelling, petrological studies of rock samples and geochemical analysis of fluids in the water column, will bring understanding of the Mayotte sismo-volcanic crisis and regional tectonics. On-going work using machine learning picking algorithms should provide a much more complete catalogue of the seismicity.

DATA AND RESOURCES

RA network (Résif 1995) YTMZ and MILA stations data available from Résif data centre (http://seismology.resif.fr). ED network MCHI station data is available upon request at EduSismo. 1T (Feuillet, Van der Woerd and RESIF, 2022) land stations are from the Résif-Sismob pool of instruments and data available upon request at Résif data centre (Péquegnat *et al*. 2021).

The INSU-IPGP pool of OBS is managed and operated by IPGP and CNRS (https://parc-obs.insu.cnrs.fr/). MicrOBS and LotOBS are operated by IFREMER/Ressources physiques et Ecosystèmes de fond de Mer/département de Géosciences Marines/service de Cartographie et Traitement de Données d'Instrumentation. Data are available upon request at IPGP data centre (http://datacenter.ipgp.fr).

AM network (Raspberry Shake Community *et al*. 2016) R0CC5, R1EE2 and RAE55 stations data are acquired by Raspberry Shake SA company and made available from IRIS data centre and Raspberry Shake SA data centre.

ObsPy (Beyreuther *et al*. 2010) was used to convert NonLinLoc results into QuakeML files. GMT (Wessel *et al*. 2019) was used for fig. 1 and fig. 6. Matlab was used for fig. 4 and fig. 5.

NonLinLoc software was used for earthquake locations with OBS data. Hypo71 software was used for preliminary earthquake locations of the first MAYOBS1 data set. VirtualBox software was used on all analyst's computer to run SeisComP3 graphical user interface client.

Lcheapo software (https://github.com/WayneCrawford/lcheapo) was used to pre-process OBS data (clock correction and conversion to miniSEED).

Past felt earthquakes statistics on Mayotte from SisFrance database: http://www.sisfrance.net.

Map bathymetry from Mayobs1 (doi:10.17600/18001217), part of the Mayobs set of cruises (doi:10.18142/291). Data available upon request at SISMER.

ACKNOWLEDGEMENTS

The Tellus SISMAYOTTE project (broad-band land stations and first OBSs, MAYOBS1, doi:10.17600/18001217) was funded by INSU,CNRS and the Ministry of Environment (ministère de la transition écologique et solidaire—MTES). Since June 2019, all activities on Mayotte are monitored by REVOSIMA (Réseau de surveillance volcanologique et sismologique de Mayotte) and funded by the Ministère de la Transition Ecologique (MTE), the Ministère de l'Enseignement Supérieur, de la Recherche et de l'Innovation (MESRI), the Ministère des Outre-Mer (MOM) and the Ministère de l'Intérieur (MI) with the support of the DIRMOM (Direction Interministérielle aux Risques Majeurs en Outremer).

All marine operations are performed as part of the MAYOBS set of cruises (Feuillet *et al*. 2019).

The MCHI station (Sismo à l'Ecole, http://edumed.unice.fr/fr) was installed by Didier Bertil and Alison Colombain, with funding from BRGM, DEAL-Mayotte and Rectorat de Mayotte.

The RaspBerry Shake instruments were installed by Maxime Bès de Berc, Marc Grunberg, Christophe Sira and Antoine Schlupp.

The Mayotte stations were installed by Maxime Bès de Berc, Jérôme van der Woerd, Céleste Broucke, Alison Colombain, Hélène Jund and Grégoire Dectot. The Grande Glorieuse station was installed by Aline Peltier and Philippe Kowalski. They are maintained by CNRS/EOST/IPGS, BRGM and OVPF-IPGP through the REVOSIMA.

OBS are deployed, recovered, maintained and data pre-processed by Romuald Daniel, Simon Besançon, Wayne Crawford and Jérémy Gomez.

MicrOBS are deployed, recovered, maintained and data pre-processed by Pascal Pelleau, Pierre Guyavarch and Mickaël Roudault.

JMS wrote the first draft of the manuscript and led the editing work. All co-authors discussed and corrected the manuscript. CA and WC provided English language check and editing. EJ compiled geological information and bibliography to establish candidate velocity models, and made figures. CS gave NonLinLoc and Python support and expertise. All co-authors participated either in station maintenance and deployment, in routine manual earthquake analysis from land network or in the different pickathons to manually pick the earthquakes. NF, YF, SJ, ER and IT led the different Mayobs cruises and helped for data interpretation.

This is IPGP contribution 4238.

REFERENCES

Beauducel, F. *et al.*, 2020. WebObs: The Volcano Observatories Missing Link Between Research and Real-Time Monitoring, *Frontiers in Earth Science,* **8,** 48, doi:10.3389/feart.2020.00048.

Bertil, D. *et al.*, 2019. MAYEQSwarm2019: BRGM earthquake catalogue for the Earthquake Swarm located East of Mayotte, 2018 May 10th–2019 May 15th, doi:10.18144/rmg1-ts50.

Bertil, D. & Regnoult, J. M., 1998. Seismotectonics of Madagascar, *Tectonophysics,* **294,** 57–74, doi:10.1016/S0040-1951(98)00088-2.

Bertil, D., Roullé, A., Lemoine, A., Colombain, A., Maisonhaute, E. & Dectot, G., 2018. MAYEQSwarm2018: BRGM earthquake catalogue for the Earthquake Swarm located East of Mayotte, May 10th–November 12th 2018, doi:10.18144/372c5809-3d30-440c-b44a-1c89385f176a.

Bès de Berc, M., Pestourie, R., Jund, H. & Broucke, C., 2019. *A Complete Characterization of 27 OSOP Raspberryshakes Performed at EOST Seismic Instrumentation Facility, Poster X2.463, EGU2019-1660,* EGU General Assembly.

Beyreuther, M., Barsh, R., Krisher, L., Megies, T., Behr, Y. & Wassermann, J., 2010. ObsPy: a Python toolbox for seismlogy, *Seismol. Res. Lett.,* **81,** 530–533, doi:10.1785/gssrl.81.3.530.

Bratt, S.R. & Bache, T.C., 1988. Locating events with a sparse network of regional arrays, *Bull. seism. Soc. Am.,* **78**(2), 780–798.

Briole, P., 2018. Note sur la crise tellurique en cours à Mayotte, mayotte_note_deformation_GPS_20181126.pdf.

Cesca, S. *et al.*, 2020. Drainage of a deep magma reservoir near Mayotte inferred from seismicity and deformation, *Nat. Geosci.,* **13,** 87–93, doi:10.1038/s41561-019-0505-5.

Chatelain, J.L., 1978. *Étude fine de la sismicité en zone de collision continentale au moyen d'un réseau de stations portables : la région Hindu-Kush Pamir, Thèse de 3eme cycle,* Université de Grenoble, 219 pp, https://tel.archives-ouvertes.fr/tel-00683028.

Coffin, M.F., Rabinowitz, P.D. & Houtz, R.E., 1986. Crustal structure in the Western Somali Basin, *Geophys. J. Int.,* **86,** 331–369.

Dofal, A., Fontaine, F., Michon, L., Barruol, G. & Hrvoje, T., 2018. Crustal structure variation across the southwestern Indian Ocean from receiver functions determined at Ocean-Bottom Seismometers, in *Proceedings of the AGU Fall Meeting,* 2018AGUFM.T43G0497B, AGU.

Dofal, A., Fontaine, F., Michon, L., Barruol, G. & Hrvoje, T., 2021. Nature of the crust beneath the islands of the Mozambique Channel: constraints from receiver functions, *J. Afr. Earth Sci.,* **184,** doi:10.1016/j.jafrearsci.2021.104379.

Duputel, Z., Lengliné, O. & Ferrazzini, V., 2019. Constraining spatiotemporal characteristics of magma migration at Piton de la Fournaise volcano from pre-eruptive seismicity, *Geophys. Res. Lett.,* **46**(1), 119–127, doi:10.1029/2018GL080895.

Dziewonski, A. M., Chou, T.-A. & Woodhouse, J. H., 1981. Determination of earthquake source parameters from waveform data for studies of global and regional seismicity, *J. geophys. Res.,* **86,** 2825–2852, doi:10.1029/JB086iB04p02825.

Ekström, G., Nettles, M. & Dziewonski, A. M., 2012. The global CMT project 2004–2010: centroid-moment tensors for 13,017 earthquakes, *Phys. Earth planet. Inter.,* **200-201,** 1–9.

Feuillet, N. *et al.*, 2021. Birth of a large volcanic edifice through lithosphere-scale dyking offshore Mayotte (Indian Ocean), *Nat. Geosci.,* **14,** 787–795 , doi:10.1038/s41561-021-00809-x.

Feuillet, N., 2019. MAYOBS1 cruise, RV Marion Dufresne, doi:10.17600/1801217.

Feuillet, N., Jorry, S., Rinnert, E., Thinon, I. & Fouquet, Y., 2019, MAYOBS set of cruises, doi:10.18142/291.

Feuillet, N. & Van der Woerd, J., RESIF. 2022. *Seismic sequence monitoring on land and at sea in Mayotte: SISMAYOTTE (RESIF-SISMOB) [Data set],* RESIF - Réseau Sismologique et géodésique Français, doi:10.15778/resif.1t2018.

Grandin, R. *et al.*, 2011. Seismicity during lateral dike propagation: Insights from newdata in the recent Manda Hararo–Dabbahu rifting episode(Afar, Ethiopia). *Geochemistry, Geophysics, Geosystems,* **12**(4), doi:10.1029/2010GC003434.

Grevemeyer, I. *et al.*, 2019. Constraining the maximum depth of brittle deformation at slow- and ultraslow-spreading ridges using microseismicity, *Geology,* **47**(11), 1069–1073, doi:10.1130/G46577.1.

International Seismological Centre, 2020. On-line Bulletin, doi:10.31905/D808B830.

Jacques, E. *et al.*, 2019. The 2018–2019 Mayotte seismic crisis: evidence of an upper mantle rifting event?, in *Proceedings of the AGU Fall Meeting 2019, 2019AGUFM.V43l0221J,* AGU.

Jacques, E., Ruegg, J.-C., Lépine, J.-C., Tapponnier, P., King, G. C. P. & Omar, A.,1999. Relocation of M ≥ 2 events of the 1989 Dôbi seismic sequence in Afar: evidence for earth- quake migration, *Geophys. J. Int.,* **138**(2), 447–469, doi:10.1046/j.1365-246X.1999.00881.x.

Kennett, B.L.N. & Engdahl, E.R., 1991. Traveltimes for global earthquake location and phase identification, *Geophys. J. Int.,* **105**(2), 429–465, doi:10.1111/j.1365-246X.1991.tb06724.x.

Kennett, B.L.N., Engdahl, E.R. & Buland, R., 1995. Constraints on seismic velocities in the Earth from traveltimes, *Geophys. J. Int.,* **122,** 108–124, doi:10.1111/j.1365-246X.1995.tb03540.x.

Lahr, J.C., 2012. HYPOELLIPSE: a computer program for determining local earthquake hypocentral parameters, magnitude, and first-motion pattern, U.S. Geological Survey Open-File Report 99–23, version 1.1, 119 pp. and software, available at, https://pubs.usgs.gov/of/1999/ofr-99-0023/.

Lambert, J., 1997. Contribution au relevé de la sismicité historique des îles de la Réunion, de Maurice et des Comores, BRGM R39763, 56p.

Lee, W.H.K. & Lahr, J.C., 1972. HYPO71: a computer program for determining hypocenter, magnitude, and first motion pattern of local earthquakes, Open-File Report, US Geological Survey, doi:10.3133/ofr72224.

Lemoine, A. *et al.*, 2020a. The 2018–2019 seismo-volcanic crisis east of Mayotte, Comoros islands: seismicity and ground deformation markers of an exceptional submarine eruption, *Geophys. J. Int.,* **223,** 22–44, doi:10.1093/gji/ggaa273.

Lemoine, A. *et al.*, 2020b. Scénarios d'impacts des tsunamis pour Mayotte – Rapport final, BRGM/RP-69869-FR, 169 p., 61 ann.

Lomax, A., Michelini, A. & Curtis, A., 2014. Earthquake location, direct, global-search methods, in *Encyclopedia of Complexity and Systems Science,* pp. Springer, 1–33.

Orcutt, J. & Constable, S., 1996. *Seafloor Data Loggers. Phase 1,* SCRIPPS Institution of Oceanography La Jolla CA, 1996.

Péquegnat, C. *et al.*, 2021. RÉSIF-SI: a distributed information system for French seismological data, *Seismol. Res. Lett.,* **92**(3), 1832–1853, doi:10.1785/0220200392.

Péquegnat, C., Guéguen, P., Hatzfeld, D. & Langlais., M., 2008. The French Accelerometric Network (RAP) and National Data Centre (RAP-NDC), *Seismol. Res. Lett.,* **79,** 79–89.

Poulain, P. *et al.*, 2021. Numerical simulation of submarine landslide and generated tsunamis: application to the Mayotte seismo-volcanic crisis, in *Proceedings of the vEGU21: The 23rd EGU General Assembly,* Copernicus Meetings, held online 19–30 April, 2021, id.EGU21-2854.

Raspberry Shake Community; OSOP, S.A.; Gempa GmbH., 2016, doi:10.7914/SN/AM.

Résif., 1995. Résif-RAP French Accelerometric Network, Résif - Réseau Sismologique et géodésique Français, doi:10.15778/RESIF.RA.

REVOSIMA, 2019. *Bulletin de l'activité sismo-volcanique à Mayotte,* Technical Report ISSN: 2680-1205, IPGP/BRGM/IFREMER/CNRS. Available online at: www.ipgp.fr/revosima.

Richter, C.F. 1958. *Elementary Seismology,* W.F. Freeman and Company and Bailey Bros. & Swinfen Ltd., 342pp.

Rindraharisaona, E.J., Tilmann, F., Yuan, X., Rümper, G., Giese, J., Rambolamanana, G. & Barruol, G., 2017. Crustal structure of southern Madagascar from receiver functions and ambient noise correlation: implications for crustal evolution: crustal structure of southern Madagascar, *J. geophys. Res.,* **122**(2), 1179–1197, doi:10.1002/2016JB013565.

Satriano, C. *et al.*, 2019. Source process of the very low frequency earthquakes during Mayotte 2018-2019 seismo-volcanic crisis, in *Proceedings of the AGU Fall Meeting 2019,* AGU.

Saurel, J.M. *et al.*, 2019. High resolution onboard manual locations of Mayotte seismicity since March 2019, using local land and seafloor stations, in *Proceedings of the AGU Fall Meeting 2019, 2019AGUFM.V43l0220S,* AGU.

Saurel, J.M. *et al.*, 2021. *2019-02-25 to 2020-05-10 Mayotte eruption earthquake catalog relocated with OBS,* doi:10.18715/IPGP.2021.kq136bzh.

Sira, C., Schlupp, A., Bontemps, M., Regis, E. & Van der Woerd, J., 2018. Essaim sismique à l'est de Mayotte, Analyse pour la période du 10 mai au 15 juin 2018, Note préliminaire du BCSF-RENASS, BCSF-RENASS2018-R4, 62 pages, 4 tableaux, 47 Fig., 5 annexes.

Storchak, D.A. *et al.*, 2017. Rebuild of the Bulletin of the International Seismological Centre (ISC), part 1: 1964–1979, *Geosci. Lett.,* **4,** 32, doi:10.1186/s40562-017-0098-z.

Urhammer, R.A. & Collins, E. R. 1990. Synthesis of Wood-Anderson seismograms from broadband digital records, *Bull. seism. Soc. Am.,* **80**(3), 702–716.

Virieux, J., 2000. Educational Seismological Project: EDUSEIS, *Seismol. Res. Lett.,* **71**(5), 530–535, doi:10.1785/gssrl.71.5.530.

Weber, B. *et al.*, 2007: SeisComP3 - automatic and interactive real time data processing, in *Proceedings of the General Assembly European Geosciences Union,* **9,** Geophysics Research Abstracts, Vol. Vienna, Austria.

Wessel, P., Luis, J.F., Uieda, L., Scharroo, R., Wobbe, F., Smith, W.H.F. & Tian, D., 2019. The Generic Mapping Tools Version 6, *Geochem. Geophys. Geosyst.,* **20,** 5556–5564, doi:10.1029/2019GC008515.

White, R. A. & McCausland, W. A., 2019. A process-based model of pre-eruption seismicity patterns and its use for eruption forecasting at dormant stratovolcanoes, *J. Volc. Geotherm. Res.,* **382,** 267–297, doi:10.1016/j.jvolgeores.2019.03.004.

SUPPORTING INFORMATION

Supplementary data are available at *GJI* online.

Table S1: ADofal gradient velocity layer model.
Table S2: Coffin449 constant velocity layer model.
Table S3: ak135 constant velocity layer model.
Figure S1a: MOCE (centre) station showing delay of approximately 0.5 s.
Figure S1b: MONE (northeast) station in the abyssal plain, showing delay of approximately 1 s.
Figure S1c: MONN (north) station, showing delay of approximately 0.5 s.
Figure S1d: MONO (northwest) station, showing delay of approximately 0.75 s.
Figure S1e: MOSE (southeast) station, showing delay of approximately 0.5 s.
Figure S1f: MOSO (southwest) station, showing a complex conversion response with possible multiple conversions and a first delay of 0.5s.
Figure S2: (a) and (b): Map and cross-section of this study catalogue (OBS locations with hybrid ADofal velocity model). (c) and (d): Map and cross-section of the same earthquakes from Lemoine *et al*. (2020a) catalogue with land-based seismic stations.
Figure S3: map of the $\log_{10}$ density of earthquakes. Density calculated using QGis heatmap plugin, a 0.01° radius and uniform kernel. The Proximal cluster, which has a donut shape, appears to have a high density of events in its northeast side.

Please note: Oxford University Press is not responsible for the content or functionality of any supporting materials supplied by the authors. Any queries (other than missing material) should be directed to the corresponding author for the paper.